PCCP

Accepted Manuscript

ROYAL SOCIETY OF CHEMISTRY

www.rsc.org/pccp

Journal Name

RSCPublishing

ARTICLE

Very low amount of TiO_2 on N-doped carbon nanotubes significantly improve oxygen reduction activity and stability of supported Pt nanoparticles

Cite this: DOI: 10.1039/xoxxoooooox

Received ooth January 2012,
Accepted ooth January 2012

DOI: 10.1039/xoxxoooooox

www.rsc.org/

Anqi Zhao,[a] Justus Masa[b] and Wei Xia*[a]

Electrochemical corrosion is a major problem for carbon materials used in electrocatalysis. Highly dispersed TiO_2 was deposited on O-functionalized and N-doped carbon nanotubes by chemical vapour deposition to tackle the carbon corrosion problem. Very low Ti loadings of about 1 wt.% were applied to minimize the negative influence of TiO_2 as a semiconductor on the high conductivity of carbon materials. Both N doping and TiO_2 coating facilitate strong metal-support interactions and favour the formation of small Pt particles. N doping improved the intrinsic catalytic activity of the carbon support and enhanced the conductivity due to the removal of surface oxygen groups, while the negative effect of TiO_2 on conductivity is counterbalanced by its promoting effect on metal-support interactions leading to enhanced overall catalytic performance. Pt/TiO_2/NCNT showed the highest ORR activity, and significantly outperformed Pt/NCNT in electrochemical stability tests.

Introduction

The electrocatalytic oxygen reduction reaction (ORR) is a major challenge for the application of fuel cells. Pt/C as the state-of-the-art electrocatalyst suffers from stability problems during long-term operation due to carbon corrosion and insufficient metal-support interactions.[1] The corrosion of carbon is often caused by surface oxidation, for example, by H_2O_2 produced as intermediate during the ORR.[2, 3] The decomposition of surface oxygen species under reaction conditions leads to the removal of surface carbon atoms, and new oxygen species can form on the carbon surface subsequently. Metal species on carbon surfaces can enhance the rate of corrosion of carbon by catalyzing the decomposition of surface oxygen groups.[4] Alternatively, metal species like Pt also catalyze the oxidation of carbon black and promote the formation of surface oxygen species.[5, 6] Hence, metal species accelerate carbon corrosion by driving oxygen reactions in both directions. As to metal-support interactions, a strong interaction is often preferred in catalysis. On the one hand, the electronic structure of supported metal particles can be modified by the strong interaction and on the other hand, strong interactions can reduce the mobility of supported metal nanoparticles and prevent them from sintering.

The degradation of carbon is a major cause for the loss of the active surface area of carbon-supported Pt catalysts, which occurs through migration/agglomeration or dissolution (and possible re-deposition) of Pt.[7-9] Hence, it is necessary to search for alternative supports that are resistant against electrochemical corrosion and stable over a sufficiently long period of time. Furthermore, it is highly desirable to find support materials that promote strong metal-support interactions, which can improve the stability of Pt nanoparticles and modify their electronic structure favorably for electrocatalysis. Nevertheless, the electronic conductivity and surface area of the support should not be compromised.

TiO_2 is an interesting candidate as support for Pt due to its high corrosion resistance.[10] As an oxide, TiO_2 favors strong metal-support interactions.[11] However, the intrinsic conductivity of TiO_2 as a semiconductor is insufficient for electrocatalysis. Although the conductivity of TiO_2 can be improved by introducing oxygen vacancies[12] or doping with nitrogen,[13] it is still significantly lower than carbon materials. Recently, carbon-coated anatase TiO_2 was used as support for Pt nanoparticles used in the ORR.[14, 15] However, the carbon-dominated surface of the composite did not address the above-mentioned major problems with carbon materials.

Carbon nanotubes (CNTs) have proved to be a promising support material in electrocatalysis due to their unique structure and superior conductivity.[16-18] Nitrogen-doped CNTs (NCNTs) used as noble metal-free electrocatalysts exhibited superior activities in the ORR under alkaline conditions.[19, 20] The doping with nitrogen can be achieved by various methods with NH_3 post-treatment as the most common one.[21] When used as support NCNTs promote metal dispersion[22] and modify the electronic structure of support nanoparticles.[23] Pt nanoparticles on NCNTs exhibited a high catalytic activity for the ORR, which was attributed to strong metal-support interactions between Pt and N.[24] Very recently, the composite of NCNTs and mesoporous TiO_2 was used as support for Pt, and accelerated stress tests disclosed that the catalyst was more stable than Pt/C in the ORR under acidic conditions.[25]

In this work, highly dispersed TiO_2 with about 1 wt.% Ti loading was coated on oxygen-functionalized and nitrogen-doped CNTs, and the obtained composite was used as support for Pt nanoparticles used in the ORR under acidic conditions.

Pt/TiO_2/NCNT showed a higher ORR activity than Pt/NCNT and superior long-term stability compared to both Pt/NCNT and standard commercial Pt/C catalyst.

Experimental

TiO_2 coating on CNTs

As-received CNTs (inner diameter 2-6 nm, outer diameter 13-16 nm, BET surface area 280 m^2 g^{-1}, Bayer AG, Leverkusen, Germany) were purified by washing in 1.5 M HNO_3 under stirring for 72 h at room temperature to remove the residual growth catalysts used in their synthesis. The acid-washed CNTs were then functionalized by HNO_3 vapor treatment at 200 °C for 72 h to introduce oxygen-containing functional groups.[26] Nitrogen-doped CNTs (NCNTs) were obtained by post-treatment of the oxygen-functionalized CNTs (OCNTs) at 600 °C for 6 h under flowing ammonia (10 vol % NH_3 in He) at a flow rate of 50 sccm. The obtained OCNTs and NCNTs were used as substrates for the deposition of TiO_2.

The deposition of TiO_2 on OCNTs and NCNTs was achieved by chemical vapor deposition in a fixed-bed reactor using $TiCl_4$ (≥ 99.0%, Fluka) as Ti precursor. In a typical experiment, about 100 mg of OCNTs or NCNTs were loaded into a vertical quartz tube reactor, and 20 µl of $TiCl_4$ were added into the sublimation chamber under helium flow at room temperature. The reactor was heated to 200 °C at 10 K min^{-1} using a resistance heating wire, and the sublimation chamber was heated to 60 °C in an oven. Simultaneously, helium (purity 99.9999%, 25 sccm) was passed through the sublimation chamber and synthetic air (20.5% O_2 in N_2, 25 sccm) was introduced to the reactor. The sublimation finished within about 1 h as indicated by an online mass spectrometer. Subsequently, the reactor was heated to 300 °C at 10 K min^{-1} under the same flow conditions, and the sample was calcined for 2 h before cooling to room temperature. The flow rates were adjusted by mass flow controllers. The obtained TiO_2-coated CNT samples are denoted as TiO_2/OCNT and TiO_2/NCNT, respectively.

Deposition of Pt nanoparticles

Colloidal Pt nanoparticles were synthesized by a modified ethylene glycol method.[27] In a typical experiment, 0.45 g of $H_2PtCl_6 \times 6H_2O$ (Aldrich) were dissolved in 250 ml of ethylene glycol (99.8%, Aldrich). A solution of NaOH in ethylene glycol (1.0 M) was dropped into the H_2PtCl_6 solution until the pH reached 12. The obtained mixture was stirred at room temperature for 24 h, and then refluxed at 160 °C for 3 h in an inert atmosphere. The obtained dark brown Pt colloid was stored at room temperature in air for further applications.

For the deposition of Pt, 200 mg of the support materials (OCNTs, NCNTs, TiO_2/OCNT and TiO_2/NCNT) were mixed with 40 ml of the Pt colloid, and the pH of the mixture was adjusted to 2 by adding 1.0 M HCl in ethylene glycol. The mixture was refluxed at 160 °C for 1.5 h before cooling to room temperature. After filtration, washing with ethanol, and drying at 60 °C in air, the obtained catalysts were reduced at 300 °C for 1 h under flowing hydrogen and were ground in an agate mortar before further tests. A commercial Pt/C catalyst purchased from E-TEK was used for comparison.

Characterization

X-ray diffraction (XRD) was performed using a PANalytical theta-theta powder diffractometer with a Cu Kα source. Scans were run from 10 to 80° with a step width of 0.03° and a collection time of 20 s per step. Elemental analysis was carried out with an ICP-OES instrument (PU701) from Philips-Unicam. X-ray photoelectron spectroscopy (XPS) measurements were carried out in an ultra-high vacuum (UHV) set-up equipped with a monochromatic Al Kα X-ray source (1486.6 eV; anode operating at 14.5 kV and 45 mA) and a high resolution Gammadata-Scienta SES 2002 analyzer. The base pressure in the measurement chamber was maintained at about 7×10^{-10} mbar. The XP spectra were recorded in the fixed transmission mode with a pass energy of 200 eV resulting in an overall energy resolution better than 0.5 eV. Charging effects were compensated by applying a flood gun.

Electrochemical tests

Electrochemical measurements were performed in a conventional three-electrode cell using glassy carbon (Ø 4 mm; HTW, Germany) modified with the catalysts as the working electrode, Ag/AgCl/3 M KCl as the reference electrode and platinum as the counter electrode. The reference electrode was calibrated with respect to the reversible hydrogen electrode (RHE). Prior to the experiments, the glassy carbon electrode was polished on polishing cloth using different alumina pastes (3.0–0.05 µm) to obtain a mirror-like surface followed by ultrasonic cleaning in water. For preparation of the working electrode, 5.0 mg of the catalyst were dispersed ultrasonically for 30 min in a mixture of water (490 µl), ethanol (490 µl) and Nafion® (5 %, 20 µl). 5.3 µl of the resulting catalyst suspension were dropped onto a polished glassy carbon electrode to obtain a catalyst loading of 210 µg cm^{-2}. The electrode was dried in air at room temperature before the measurements.

Cyclic voltammetry (CV) and linear sweep voltammetry (LSV) measurements were carried out in aqueous 0.1 M $HClO_4$ using an Autolab potentiostat/galvanostat (PGSTAT12, Eco Chemie, Utrecht, The Netherlands). All oxygen reduction experiments were carried out at room temperature at a scan rate of 10 mV s^{-1} after purging the electrolyte with argon or oxygen for 20 min. Before each measurement, the catalyst was scanned in Ar-saturated electrolyte and the obtained background voltammogram was subtracted from the one recorded in the O_2-saturated electrolyte.

Results and discussion

The TiO_2 coating on CNTs was achieved by chemical vapor deposition, which is especially suitable for deposition of thin films or nanoparticles of low loadings. The XRD patterns of the TiO_2/OCNT and TiO_2/NCNT samples are shown in Figure 1. Only three diffraction peaks can be observed at about 26.0, 42.8 and 53.3°, which can be assigned to the (002), (100)/(101) and (004) reflections of functionalized CNTs, respectively.[28] The peaks shifted slightly to smaller 2θ in comparison to graphite due to the slight distortion caused by the introduction of oxygen and nitrogen atoms as well as defects in the carbon lattice.[29, 30] Diffraction peaks of TiO_2 of any polymorphs were not detected indicating that the TiO_2 coating was below the XRD detection limit due to the small crystallite size. Similar results were observed for TiO_2 deposited on silica, where TiO_2 appeared to be in form of a thin film or islands.[31]

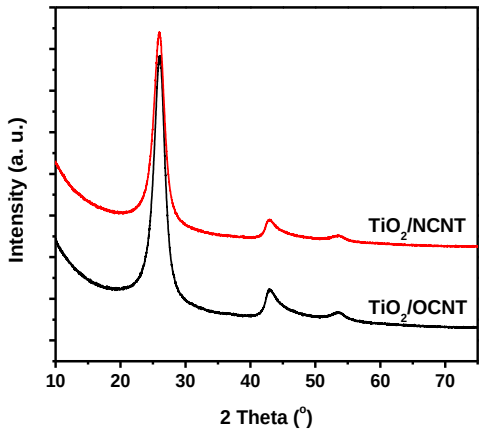

Figure 1. XRD patterns of TiO_2/OCNT and TiO_2/NCNT.

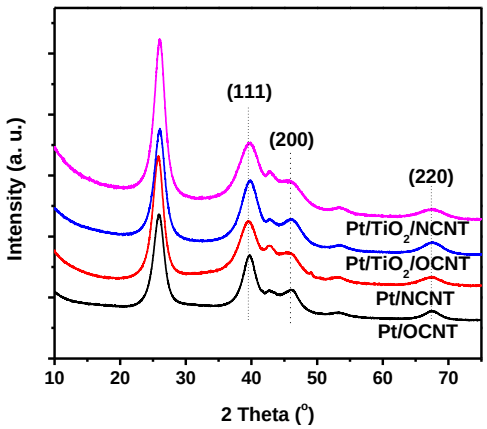

Figure 2. XRD patterns of the supported Pt catalysts with about 8 wt.% Pt loading.

After the deposition of Pt nanoparticles on the CNT and TiO_2/CNT supports, the contents of Ti and Pt in the samples were determined by ICP-OES (Table 1). The Ti contents were 1.51 wt.% and 0.94 wt.% in Pt/TiO_2/OCNT and Pt/TiO_2/NCNT, respectively. $TiCl_4$ used as precursor is highly unstable upon contact with air or water. The high yield of Ti on OCNTs is obviously related to the surface oxygen groups, which facilitate the hydrolysis of $TiCl_4$ and its conversion to TiO_2 from the gas phase. As to Pt deposited from the liquid phase, the loadings are similar on all the substrates demonstrating the high reproducibility of the colloidal method used for Pt deposition.

Table 1. Metal contents determined by elemental analysis and average Pt particle size derived from XRD studies.

Sample	Ti loading (wt.%)	Pt loading (wt.%)	d_{Pt} (nm)
Pt/OCNT	-----	7.92	7.9
Pt/NCNT	-----	7.99	5.1
Pt/TiO_2/OCNT	1.51	7.92	5.7
Pt/TiO_2/NCNT	0.94	7.95	4.8

Figure 2 shows the XRD patterns of the samples after Pt deposition. In addition to the graphitic carbon peaks, three new reflections originating from Pt nanoparticles can be observed at $2\theta = 39.8$, 46.1 and 67.7° corresponding to the characteristic Pt (111), (200) and (220) peaks, respectively.[32] The average crystallite size of the Pt nanoparticles derived by Scherrer equation using the Pt (111), (200) and (220) peaks ranged from 4.8 to 7.9 nm (Table 1). The Pt/NCNT sample exhibited smaller Pt particle sizes than the Pt/OCNT sample due to the strong interaction between Pt and N species, which is in good agreement with literature results.[22, 33] As compared to inert surface of carbon materials, oxides like TiO_2 facilitate strong metal-support interactions. Hence, the TiO_2 coating led to a decrease of the Pt particle size. Both Pt/TiO_2/OCNT and Pt/TiO_2/NCNT showed smaller Pt particle sizes than the corresponding catalysts without TiO_2, i.e., Pt/OCNT and Pt/NCNT. The smallest Pt particle size was observed for Pt/TiO_2/NCNT with both nitrogen and TiO_2 being present. The results disclose that both N and TiO_2 enable strong interactions and even a small amount on the carbon surface exhibit significant effects on supported particles.

Figure 3 shows representative scanning transmission electron microscopy (STEM) images of the four samples. It can be seen that Pt nanoparticles are homogeneously dispersed on the surface of carbon nanotubes. Corresponding size distributions of Pt nanoparticles are given in the insets. The particle size of Pt on NCNTs is smaller than that on OCNTs in accordance with the XRD results. As shown in the TEM images and Ti mapping in Figure 4, TiO_2 species are also highly dispersed on the surface of the nanotubes in Pt/TiO_2/OCNT and Pt/TiO_2/NCNT despite of its extremely low loadings in both samples.

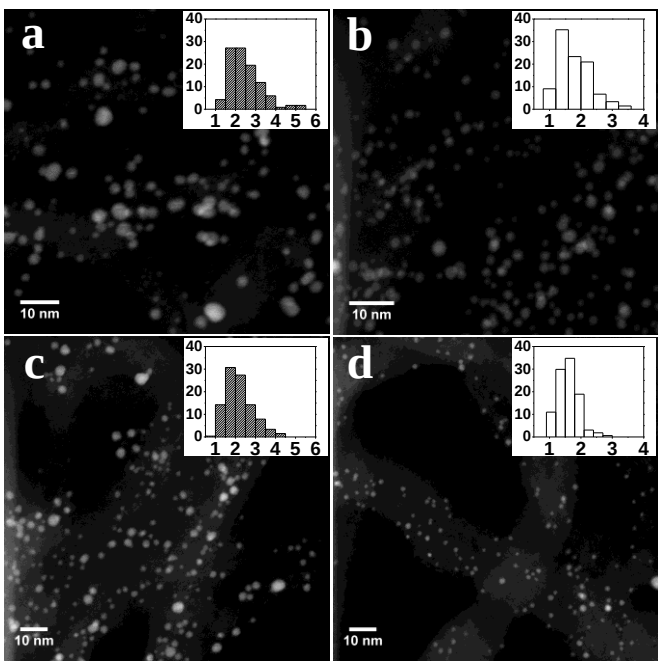

Figure 3. STEM images of Pt/OCNT (a), Pt/NCNT (b), Pt/TiO_2/OCNT (c) and Pt/TiO_2/NCNT (d). Inset: histogram of Pt particles.

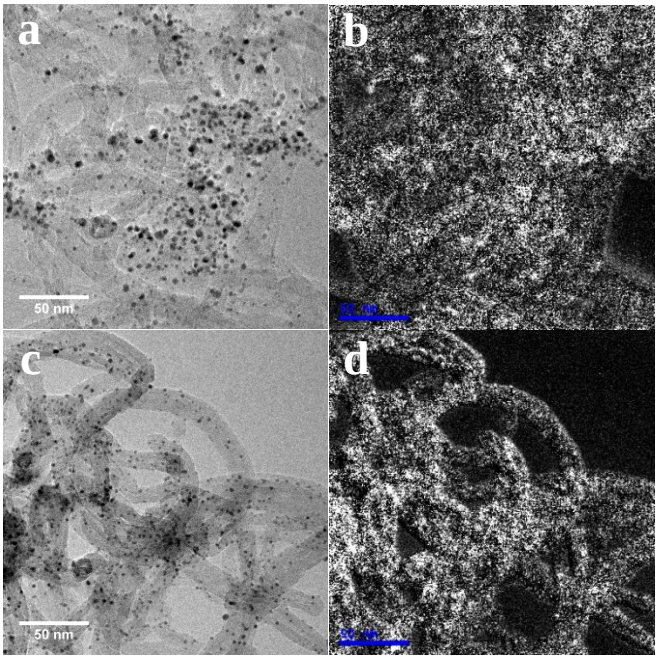

Figure 4. TEM images and corresponding Ti mapping of Pt/TiO_2/OCNT (a and b) and Pt/TiO_2/NCNT (c and d). Scale bar: 50 nm.

The surface chemistry of the samples was investigated by high-resolution XPS. In the survey spectra of the samples C, O, N, Ti and Pt were detected without other impurities. The region spectra were normalized to the intensity of the C 1s peak at 284.5 eV. The XP C 1s and O 1s spectra of all the samples were measured (not shown). No significant differences were observed in the C 1s spectra of the samples. The O 1s region composes of three major contributions including oxygen in metal oxide at 530.2 eV, oxygen in C=O at 531.2 eV and oxygen in C-O at 533.1 eV.[22, 34] Figure 5 shows the normalized N 1s spectra of Pt/NCNT and Pt/TiO_2/NCNT. It can be seen that the N 1s peak of Pt/TiO_2/NCNT is quite similar to that of Pt/NCNT with only a slight decrease in intensity. Hence, it can be assumed that the TiO_2 coating is much thinner than the escape depth of photoelectrons in XPS pointing to its high dispersion at the low Ti loading of 0.94 wt.%.

The XP Ti 2p spectra of the Pt/TiO_2/OCNT and Pt/TiO_2/NCNT samples are shown in Figure 6. The two peaks at 459.2 and 464.9 eV in both samples can be assigned to Ti $2p_{3/2}$ and Ti $2p_{1/2}$, respectively.[35, 36] The peak separation between the Ti $2p_{1/2}$ and Ti $2p_{3/2}$ lines is 5.7 eV, which is consistent with the +4 oxidation state of Ti.[37] Since the spectra are normalized, the significantly higher intensity of Ti peaks in Pt/TiO_2/OCNT than in Pt/TiO_2/NCNT can be attributed to a considerably higher Ti loading, which is in good agreement with elemental analysis. Moreover, no evident interaction between Ti and N atoms was observed in the Ti 2p spectrum of the Pt/TiO_2/NCNT sample suggesting that nitrogen species were not significantly affected by the TiO_2 coating. Figure 7 shows the XP Pt 4f spectra of the supported Pt samples. The Pt $4f_{7/2}$ and $4f_{5/2}$ peaks were observed at binding energies of 71.2 eV and 74.5 eV, respectively, with a peak separation of 3.3 eV. This result indicates that Pt is mostly in the metallic state on the supports.[38]

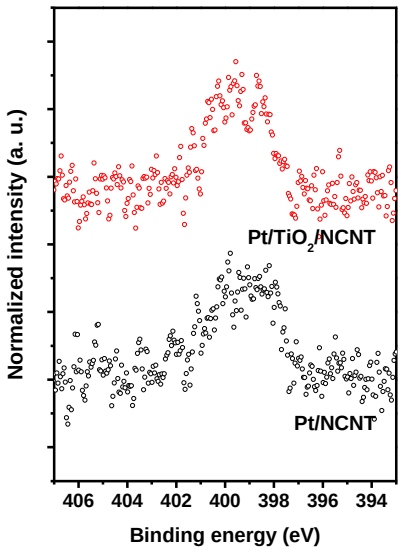

Figure 5. XP N 1s spectra of Pt/NCNT and Pt/TiO_2/NCNT.

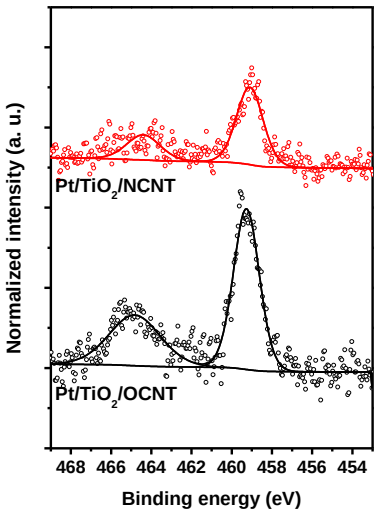

Figure 6. XP Ti 2p spectra of Pt/TiO_2/OCNT and Pt/TiO_2/NCNT.

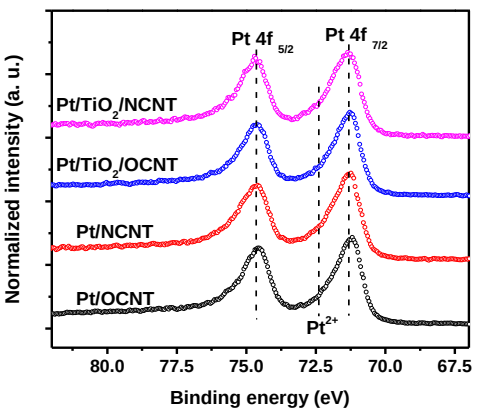

Figure 7. XP Pt 4f spectra of different catalysts.

Figure 8 shows the cyclic voltammograms of Pt in argon-saturated 0.1 M $HClO_4$ recorded at a scan rate of 100 mV s^{-1}. Characteristic Pt features were clearly visible in the voltammograms of all the samples, notably, the hydrogen adsorption and desorption peaks in the potential range from -0.05 to 0.37 V. The electrochemically active surface areas (ECSA) of Pt determined from the average of the area under the adsorption and desorption waves were 24.9 m^2/g (Pt/OCNT), 50.9 m^2/g (Pt/NCNT), 40.6 m^2/g (Pt/TiO_2/OCNT) and 42.6 m^2/g (Pt/TiO_2/NCNT). We attribute the low ECSA of Pt/OCNT compared to Pt/NCNT to the lower conductivity of OCNT compared to NCNT, and the stronger interaction between Pt and N which minimizes the agglomeration of Pt nanoparticles on NCNTs resulting in a higher dispersion of the Pt nanoparticles on NCNTs, which is consistent with the XRD and STEM results. One would expect that the deposition of TiO_2 on OCNT would lead to a lower conductivity and hence a lower ECSA of Pt/TiO_2/OCNT than Pt/OCNT. On the contrary, the ECSA of Pt/TiO_2/OCNT (40.6 m^2/g) was higher than that of Pt/OCNT (24.9 m^2/g), which can be attributed to the strong metal-support interaction in Pt/TiO_2/OCNT favoring high Pt dispersion and charge transfer.

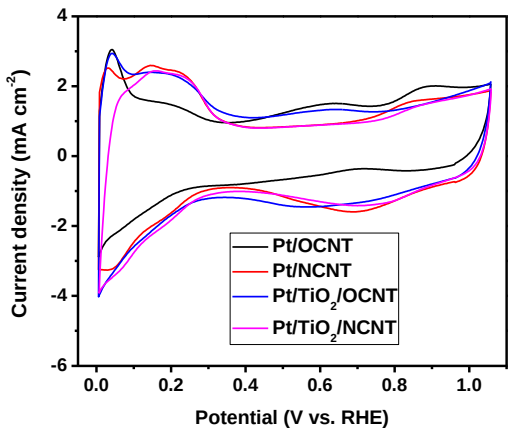

Figure 8. Cyclic voltammograms of the supported Pt catalysts measured in argon-saturated 0.1 M $HClO_4$ at a scan rate of 100 mV s^{-1}.

The electrochemical activities of the supported Pt catalysts in the ORR were investigated by linear sweep voltammetry in oxygen-saturated 0.1 M $HClO_4$. Background corrected linear sweep voltammograms recorded at 10 mV s^{-1} are shown in Figure 9. It is worth to note that a relatively low Pt loading of around 8 wt% was applied for all the samples in order to investigate the effect of the support. Due to the low loading, the samples did not show uniform diffusion limited currents. However, the difference between the samples is clearly distinguishable. Pt/OCNT exhibited the lowest ORR activity indicated by the most negative onset potential. The TiO_2 coating on OCNTs improved the ORR performance of the Pt catalysts, and the onset potential of Pt/TiO_2/OCNT is clearly higher than that of Pt/OCNT. A negative effect is often expected for the TiO_2 deposition due to its low conductivity as a semiconductor. However, thanks to the extremely low Ti loading and high dispersion, the negative effect was counterbalanced by the positive effect of the TiO_2 coating, that is, enhanced interaction with Pt and improved dispersion as well as charge transfer. Hence, the overall effect of the TiO_2 coating is positive as disclosed by the significantly improved ORR activities (Figure 9). NCNTs are expected to enhance the catalytic activity for the ORR owing to their intrinsic catalytic activity, high electronic conductivity, high dispersion of supported Pt particles and strong metal-support interactions. As expected, Pt/NCNT exhibited a higher onset potential than Pt/OCNT, and Pt/TiO_2/NCNT showed the best ORR performance as indicated by the most positive onset potential and the highest catalytic current (Figure 9). We have shown that TiO_2 in CNT/TiO_2 composites (weight ratio 1:3) caused the decrease of ORR activity while improving stability.[25] Hence, both nitrogen and TiO_2 can improve ORR activity, whereas TiO_2 improves ORR activity only at low loading and high degree of dispersion.

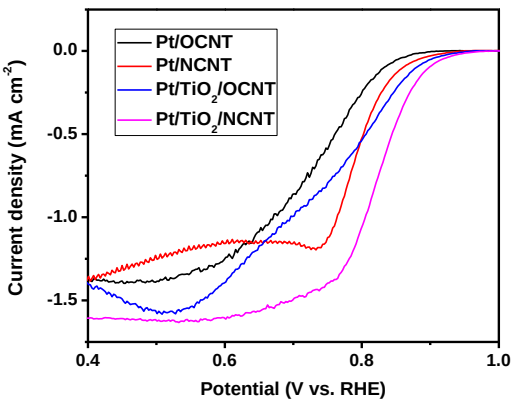

Figure 9. Linear sweep voltammograms of Pt catalysts on various supports measured in oxygen-saturated 0.1 M $HClO_4$ at a scan rate of 10 mV s^{-1} and a rotation rate of 400 rpm. A relatively low Pt loading of ca. 8wt % was applied to investigate the support effect.

Pt/NCNT and Pt/TiO_2/NCNT were selected for electrochemical stability studies and compared with a commercial Pt/C (20 wt.% Pt) catalyst. The stability measurements were carried out at a constant potential of 0.76 V for 60 h in 0.1 M $HClO_4$, which was exposed to air during the measurement. The current after the initial 5 h was set at 100 % performance for a better comparison. The corresponding current–time chronoamperometric responses are shown in Figure 10. It can be seen that Pt/NCNT exhibited a slower decrease in current than commercial Pt/C, which can be attributed to the structural difference of the supports. NCNTs with ordered graphitic structure are more stable than the amorphous carbon black. In contrast, the Pt/TiO_2/NCNT sample showed a very slow deactivation in the first 20 h and much slower decrease of reduction current in the following hours. Hence, the small amount of TiO_2 as interlayer between carbon and Pt can tremendously enhance the electrochemical stability of Pt nanoparticles on carbon supports.

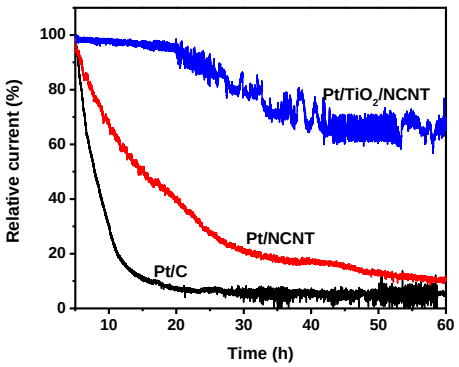

Figure 10. Current-time chronoamperometric response of Pt/NCNT, Pt/TiO_2/NCNT and commercial Pt/C at 0.76 V vs RHE in air-saturated 0.1 M $HClO_4$.

Conclusions

The coating of CNTs with highly dispersed TiO_2 was achieved by chemical vapor deposition using $TiCl_4$ as precursor. The high dispersion of TiO_2 with about 1 wt.% Ti loading was confirmed by XRD, XPS and TEM studies. Both the nitrogen doping and the TiO_2 coating facilitate strong metal-support interactions and favor the formation of small Pt nanoparticles. The doping of nitrogen improved the conductivity of the carbon support through the removal of surface oxygen groups. Nitrogen species are also intrinsically active for the ORR. Due to the low loading and high dispersion, TiO_2 as a semiconducting oxide showed only a limited negative influence on the high conductivity of carbon materials. Instead, TiO_2 exhibited a strong promoting effect by enhancing metal-support interactions. The Pt particles are smaller after nitrogen doping and TiO_2 coating. As a result, the overall ORR activity and stability under acidic conditions was enhanced by nitrogen doping and TiO_2 coating. Pt/TiO_2/NCNT showed the highest ORR activity, and significantly outperformed Pt/NCNT in electrochemical stability tests.

Acknowledgements

Anqi Zhao thanks China Scholarship Council for a research grant.

Notes and references

[a] Laboratory of Industrial Chemistry, Ruhr-University Bochum, Germany Corresponding author: Fax: +49 234 32 14115; E-mail: wei.xia@techem.rub.de

[b] Analytical Chemistry and Center for Electrochemistry, Ruhr-University Bochum, Germany

1. S. Shrestha, Y. Liu and W. E. Mustain, *Catal. Rev.*, 2011, 53, 256-336.
2. T. S. Olson, S. Pylypenko, J. E. Fulghum and P. Atanassov, *Journal of The Electrochemical Society*, 2010, 157, B54-B63.
3. J. D. Wiggins-Camacho and K. J. Stevenson, *The Journal of Physical Chemistry C*, 2011, 115, 20002-20010.
4. C. Jin, W. Xia, P. Chen and M. Muhler, *Catal. Today*, 2012, 186, 128-133.
5. L. M. Roen, C. H. Paik and T. D. Jarvi, *Electrochem. Solid-State Lett.*, 2004, 7, A19-A22.
6. K. H. Kangasniemi, D. A. Condit and T. D. Jarvi, *J. Electrochem. Soc.*, 2004, 151, E125-E132.
7. Y. Shao-Horn, W. C. Sheng, S. Chen, P. J. Ferreira, E. F. Holby and D. Morgan, *Top. Catal.*, 2007, 46, 285-305.
8. R. Borup, J. Meyers, B. Pivovar, Y. S. Kim, R. Mukundan, N. Garland, D. Myers, M. Wilson, F. Garzon, D. Wood, P. Zelenay, K. More, K. Stroh, T. Zawodzinski, J. Boncella, J. E. McGrath, M. Inaba, K. Miyatake, M. Hori, K. Ota, Z. Ogumi, S. Miyata, A. Nishikata, Z. Siroma, Y. Uchimoto, K. Yasuda, K. I. Kimijima and N. Iwashita, *Chem. Rev.*, 2007, 107, 3904-3951.
9. J. C. Meier, C. Galeano, I. Katsounaros, A. A. Topalov, A. Kostka, F. Schüth and K. J. J. Mayrhofer, *ACS Catal.* , 2012, 2, 832-843.
10. S. Shanmugam and A. Gedanken, *J. Phys. Chem. C*, 2009, 113, 18707-18712.
11. A. G. Dylla and K. J. Stevenson, *Chemical Communications*, 2011, 47, 12104-12106.
12. J.-Y. Shin, J. H. Joo, D. Samuelis and J. Maier, *Chem. Mater.*, 2012, 24, 543-551.
13. E. Ventosa, W. Xia, S. Klink, F. L. Mantia, B. Mei, M. Muhler and W. Schuhmann, *Chem. Eur. J.*, 2013, 19, 14194-14199.
14. S. Shanmugam and A. Gedanken, *Small*, 2007, 3, 1189-1193.
15. L. Xiong and A. Manthiram, *Electrochim. Acta*, 2004, 49, 4163-4170.
16. P. J. Britto, K. S. V. Santhanam, A. Rubio, J. A. Alonso and P. M. Ajayan, *Adv. Mater.*, 1999, 11, 154-157.
17. T. Matsumoto, T. Komatsu, K. Arai, T. Yamazaki, M. Kijima, H. Shimizu, Y. Takasawa and J. Nakamura, *Chem. Commun.*, 2004, 840-841.
18. J. Zhu, A. Holmen and D. Chen, *ChemCatChem*, 2013, 5, 378-401.
19. K. Gong, F. Du, Z. Xia, M. Durstock and L. Dai, *Science*, 2009, 323, 760-764.
20. D. W. Wang and D. S. Su, *Energy & Environmental Science*, 2014, 7, 576-591.
21. C. Li, A. Zhao, W. Xia, C. Liang and M. Muhler, *J. Phys. Chem. C*, 2012, 116, 20930-20936.
22. M. D. Sánchez, P. Chen, T. Reinecke, M. Muhler and W. Xia, *ChemCatChem*, 2012, 4, 1997-2004.
23. P. R. Chen, L. M. Chew, A. Kostka, M. Muhler and W. Xia, *Catal. Sci. Technol.*, 2013, 3, 1964-1971.
24. G. Vijayaraghavan and K. J. Stevenson, *Langmuir*, 2007, 23, 5279-5282.
25. J. Masa, A. Bordoloi, M. Muhler, W. Schuhmann and W. Xia, *ChemSusChem*, 2012, 5, 523-525.
26. W. Xia, C. Jin, S. Kundu and M. Muhler, *Carbon*, 2009, 47, 919-922.
27. C. Li, Z. Shao, M. Pang, C. T. Williams and C. Liang, *Catal. Today*, 2012, 186, 69-75.
28. C.-M. Chen, Y.-M. Dai, J. G. Huang and J.-M. Jehng, *Carbon*, 2006, 44, 1808-1820.
29. L. Qu, Y. Liu, J.-B. Baek and L. Dai, *ACS Nano*, 2010, 4, 1321-1326.
30. E. N. Nxumalo and N. J. Coville, *Materials*, 2010, 3, 2141-2171.
31. W. Xia, B. Mei, M. D. Sanchez, J. Strunk and M. Muhler, *J. Nanosci. Nanotech.*, 2011, 11, 8152-8157.
32. X. Hu, H. Ji and L. Wu, *RSC Adv.*, 2012, 2, 12378-12383.
33. P. Chen, L. M. Chew and W. Xia, *Journal of Catalysis*, 2013, 307, 84-93.
34. C. Jin, T. C. Nagaiah, W. Xia, B. Spliethoff, S. Wang, M. Bron, W. Schuhmann and M. Muhler, *Nanoscale*, 2010, 2, 981-987.
35. G. Liu, W. Jaegermann, J. He, V. Sundstrom and L. Sun, *J. Phys. Chem. B*, 2002, 106, 5814-5819.
36. B. Erdem, R. A. Hunsicker, G. W. Simmons, E. D. Sudol, V. L. Dimonie and M. S. El-Aasser, *Langmuir*, 2001, 17, 2664-2669.
37. R. Sanjinés, H. Tang, H. Berger, F. Gozzo, G. Margaritondo and F. Lévy, *J. Appl. Phys.*, 1994, 75, 2945-2951.
38. P. Bera, K. R. Priolkar, A. Gayen, P. R. Sarode, M. S. Hegde, S. Emura, R. Kumashiro, V. Jayaram and G. N. Subbanna, *Chem. Mater.* , 2003, 15, 2049-2060.

